Eurographics Symposium on Rendering 2020
C. Dachsbacher and M. Pharr
(Guest Editors)

Volume 39 (2020), Number 4

Supplemental material: Practical Measurement and Reconstruction of Spectral Skin Reflectance

Y. Gitlina[1] G. C. Guarnera[2,3] D. S. Dhillon[1,4] J. Hansen[5] A. Lattas[1] D. Pai[5] A. Ghosh[1]

[1]Imperial College London [2]NTNU [3]University of York [4]Clemson University [5]UBC

1. Details of the Spectral Skin BSSRDF Model

Various terms, parameters and coefficients involved in the spectral skin BSSRDF model of [JSB*10] employed in this work are tabulated along with their descriptions in Table 1. The BSSRDF employs a mutipole model for scattering in the thin epidermis, and a dipole model for scattering in the thicker dermis. To model subsurface scattering using the multipole and dipole formulations for epidermis and dermis layers, we need to first compute their absorption and scattering coefficients.

The wavelength λ dependent spectral absorption coefficient for the epidermal layer is given as:

$$\begin{aligned}\sigma_a^{\text{epi}} = \; & C_m\left[\beta_m\sigma_a^{\text{em}}(\lambda)+(1-\beta_m)\sigma_a^{\text{pm}}(\lambda)\right] \\ & + C_{he}\left[\gamma\sigma_a^{\text{oxy}}(\lambda)+(1-\gamma)\sigma_a^{\text{deoxy}}(\lambda)\right] \\ & + (1-C_m-C_{he})\sigma_a^{\text{base}}, \end{aligned} \tag{1}$$

where, the absorption coefficients for eumelanin and pheomelanin (two types of melanin in skin) is computed as:

$$\sigma_a^{\text{em}}(\lambda) = 6.6\times10^{10}\times\lambda^{-3.33} \quad \text{mm}^{-1}, \tag{2}$$

$$\sigma_a^{\text{pm}}(\lambda) = 2.9\times10^{14}\times\lambda^{-4.75} \quad \text{mm}^{-1}, \quad \text{and} \tag{3}$$

the baseline absorption coefficient σ^{base} for the cellular matrix is defined as:

$$\sigma_a^{\text{base}}(\lambda) = 0.0244 + 8.53e^{-(\lambda-154)/66.2} \quad \text{mm}^{-1}. \tag{4}$$

Note that λ in above equations is defined is nanometers. The absorption coefficients σ_a^{oxy} and σ_a^{deoxy} for the oxygenated and deoxygenated hemoglobin are borrowed from measurements provided in medical literature [DJ06].

Similar to epidermis, the absorption coefficient for the dermal layer is defined as:

$$\sigma_a^{\text{derm}}(\lambda) = C_h\left(\gamma\sigma_a^{\text{oxy}}(\lambda)+(1-\gamma)\sigma_a^{\text{deoxy}}(\lambda)\right)+(1-C_h)\sigma_a^{\text{base}}(\lambda). \tag{5}$$

Next, the reduced scattering coefficient for the dermis is computed as:

$$\sigma_s'^{\,\text{derm}}(\lambda) = 7.37\lambda^{-0.22}+1.1\times10^{11}\times\lambda^{-4}, \quad \text{and} \tag{6}$$

Table 1: *Parameters of spectral skin BSSRDF model.*

Term	Description
λ	wavelength of light in nanometers
C_m	Melanin concentration in epidermis
C_h	Hemoglobin concentration in dermis
C_{he}	Hemoglobin concentration in epidermis
β_m	Eumelanin vs pheomelanin blend fraction in epidermis
σ_a	Layer dependent absorption coefficient
σ_s'	Layer dependent reduced scattering coefficient
γ	Ratio of oxygenated to total hemoglobin

the reduced scattering coefficient for the epidermis is given by:

$$\sigma_s'^{\,\text{epi}}(\lambda) = 14.74\lambda^{-0.22}+2.2\times10^{11}\times\lambda^{-4}. \tag{7}$$

(a) 2D model (b) Photograph (c) 4D model

Figure 1: *Comparison of facial photographs under uniform broadband (W57 cool white LED) illumination (b) to reconstructions using the reduced 2D spectral model of Jimenez et al. [JSB*10] (a), and using the complete 4D model (c).*

Using σ_a and σ_s' as absorption and reduced scattering coefficients for the dipole formulation for dermis, its reflectance profile can be computed as explained by Donner and Jensen [DJ05].

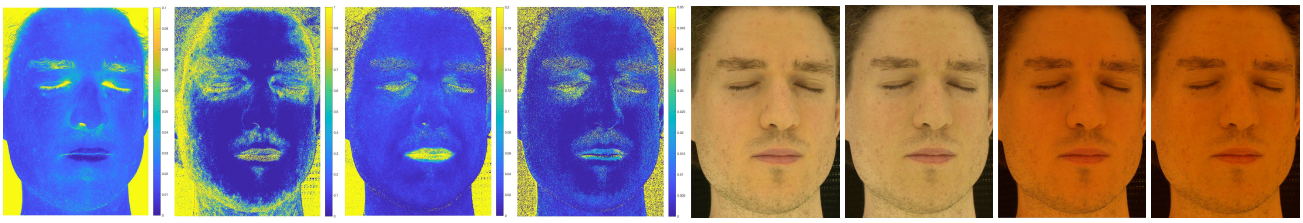

(a) C_m (b) β_m (c) C_h (d) C_{he} (e) $W57$ photo (f) $W57$ recon. (g) $W27$ photo (h) $W27$ recon.

Figure 2: *Estimated spectral parameters for a face of a Caucasian male subject, and comparison of photographs with reconstructions under different types of broadband illumination. Measurement using W57 cool white LED for broadband illumination.*

Similarly, they also explain how transmittance and reflectance profiles for the epidermis can be computed using its absorption and reduced scattering coefficients with a multipole model. These individual profiles are then convolved to compute the net reflectance profile which is then subject to surface integration to compute diffuse albedo observed due to subsurface scattering in skin. We refer the reader to Donner&Jensen [DJ06] for further details.

Figure 1 shows comparisons of facial photographs under uniform broadbad illumination, and their reconstruction using the reduced 2D spectral model employed by Jimenez et al. [JSB*10] with only two free parameters (C_m and C_h) (a), and reconstruction using the complete 4D model with two additional free parameter (β_m, and C_{he}) (c). As can be seen, the 4D model allows a closer match to the spatially varying appearance of skin in the photographs.

2. Measurements with LED Sphere

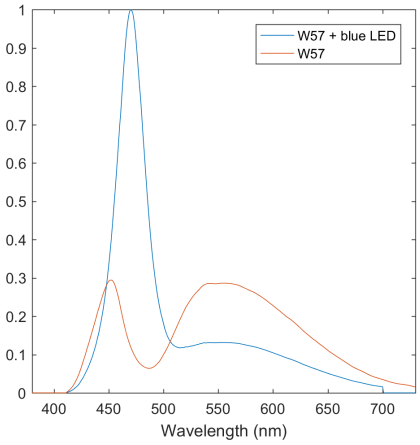

Figure 3: *Spectra of W57 and W57 + blue illumination, jointly used to isolate the blue response.*

Figures 3 and 4 show the spectra of illuminants, and the acquired photographs respectively, employed to estimate spectral parameters of a subject acquired using W57 cool white LED as the broadband in conjunction with narrow-band blue LED illumination. As can be seen, the process is very similar to the employment of D65 metamer for the broadband measurement and the estimated parameters are of sufficiently high quality to reconstruct skin appearance under different illumination spectra (see Figure 2).

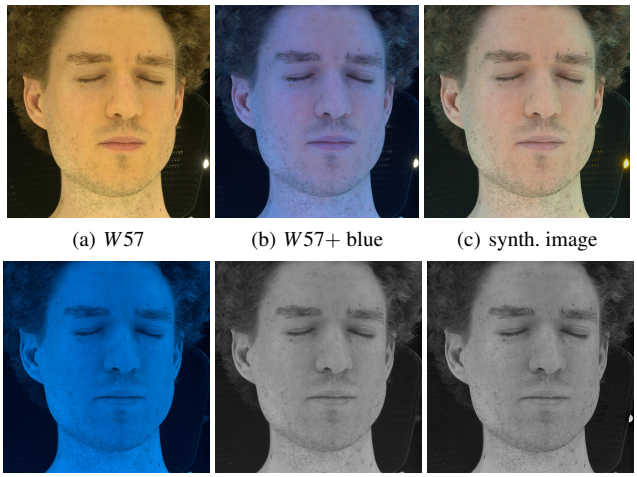

(a) $W57$ (b) $W57+$ blue (c) synth. image (d) direct blue illum. (e) direct blue isol. (f) synth. blue isol.

Figure 4: *Proposed practical spectral measurements of skin reflectance (a, b). (a) Broadband W57 illumination. (b) Mix of W57+ blue LED illumination. (c) Synthesized reponse to pure blue LED illumination, and its isolated blue channel data (f) employed for parameter estimation. (d) Direct measurement of skin response to blue illumination, and its isolated blue channel data (e).*

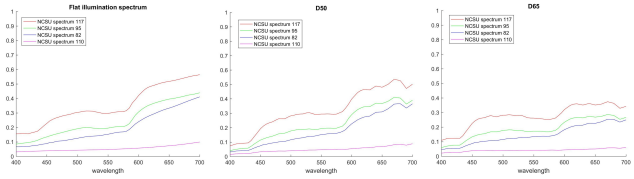

(a) skin reflectance (b) D50 response (c) D65 response

Figure 5: *Skin reflectance spectrum (from [DJ06]) and its response under: (a) Flat illumination spectrum. (b) D50 spectrum (employed by [JSB*10]). (c) D65 spectrum.*

Given the 6 types of LEDs in our LED sphere, we prefer to create an ideal broadband illumination by computing a weighted combination of all 6 LEDs to create a D65 metamer spectra ($D65'$) which we employ for our broadband measurements. We notice a higher contrast in skin color, particularly coloration due to skin pigmentation and redness, under the D65 metamer illumination compared to

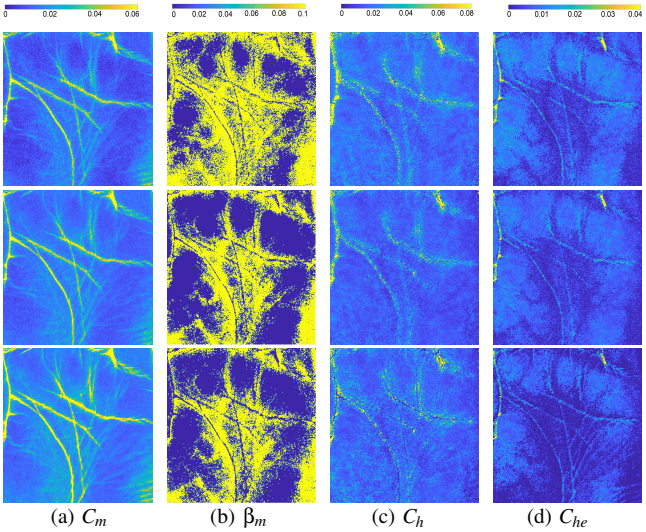

(a) C_m (b) β_m (c) C_h (d) C_{he}

Figure 6: *Estimated spectral parameters for a palm. Top-row: Using just broad band W57 LED illumination. Center-row: Estimation using D65 metamer ($D65'$) broadband illumination. Bottom-row: Joint-estimation using $D65'$ broadband + narrow band blue LED illumination.*

any of the individual white LEDs including W57. This is consistent with our observation that D65 spectrum (blue dominant) balances the somewhat skewed red-dominant reflectance spectrum of human skin (see Figure 5).

Figure 6 shows comparisons of parameter maps for a palm of a hand of a darker skin subject obtained using a single measurement under W57 illumination (top-row), vs our proposed two complementary measurements (bottom-row). As can be seen, our proposed approach of two complementary spectral measurements enables higher quality parameter estimation with less noise and clearer spatial structure of chromophore concentrations. Even for a single observation under broadband illumination, we see an improvement in the quality of estimated parameters when employing the D65 metamer illumination for the broadband measurement (center-row). Photograph-reconstruction comparisons of the palm under various illumination spectra can be seen in Figure 7.

Figure 8 shows the spectral parameter maps for the palm estimated using W57 + blue illumination (top-row), and $D65'$ + blue (bottom-row). While qualitatively very similar, the parameters in the bottom-row estimated using $D65'$ for the broadband measurement exhibit slightly reduced noise and better generalize to novel spectral illumination conditions.

For baseline measurements in the LED sphere, we also did an analysis of which type of broadband illumination is most suitable for estimating the spectral parameters of skin. Across four different skin types ranging from Caucasian, Mediterranean, Asian, and South Asian, we consistently found the reconstruction accuracy of estimation using the cold spectrum broadband illumination (W57) to be higher for reconstructing the appearance of skin under both colder and warmer broadband spectrums. And we also found a clear ordering in decreasing order of accuracy for generalization to a different illumination spectrum from W57, followed by W40, and then W27. This is why we selected the W57 as the choice for the baseline measurement. Measurements under each of these broadband condition were most accurate for reproducing the appearance under their own spectral conditions, pointing to some overfitting to the measurement spectrum. This issue is mitigated to quite an extent when we employ the D65 metamer illumination for broadband measurements, improving the generalization to a different illumination spectrum.

(a) $D65'$ (b) $W57$ (c) $W40$ (d) $W27$

Figure 7: *Photographs (top-row) vs reconstructions (bottom-row) of the palm under uniform illumination with four different spectra. The reconstructions use the estimated parameters in Figure 6 (bottom-row).*

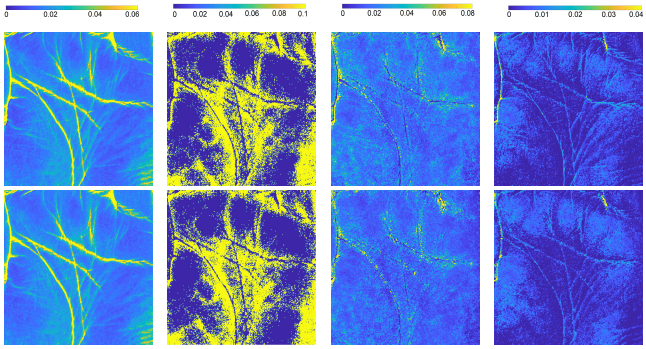

(a) C_m (b) β_m (c) C_h (d) C_{he}

Figure 8: *Comparison of estimated spectral parameters for the palm. Top-row: Using broad band W57 + narrow band blue LED illumination. Bottom-row: Joint-estimation using $D65'$ broadband + narrow band blue LED illumination.*

Table 2: *Mean DeltaE94 errors*

Sample	2D mapping	Augmented	4D Search
Cheek	3.5287	1.5501	0.3734
Forehead	4.4078	3.1809	1.5072
Back of hand	2.3648	1.344	0.2314
Palm	3.7679	2.7096	1.0483

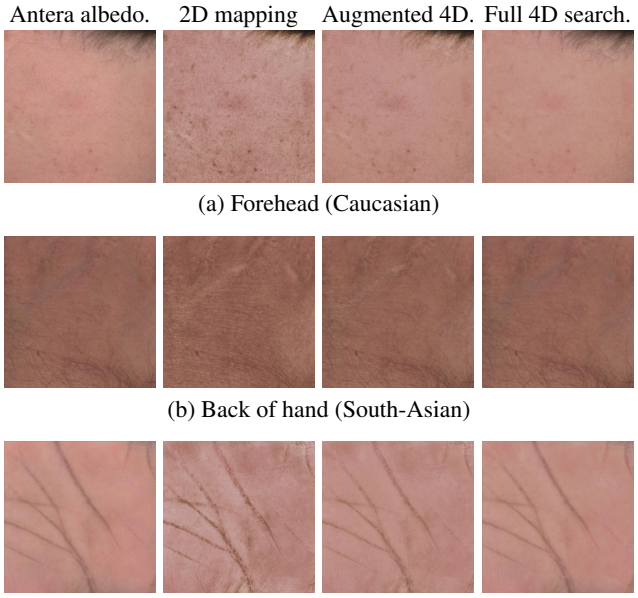

(a) Forehead (Caucasian)

(b) Back of hand (South-Asian)

(c) Palm (South-Asian)

Figure 9: *Additional examples of skin patch measurements with Antera. Center-left: Initial 2D mapping of Antera's parameters. Center-right: Adapting and augmenting Antera's parameters for the skin model. Right: Parameter estimation using full 4D search.*

3. Measurements with Antera3D

Figure 9 presents a few additional examples of skin patches that we measured using the Antera device. This includes a forehead patch of a Caucasian subject (top-row), and the back of the hand (center row), and the palm (bottom row) for a subject with darker (South Asian) skin type. For all of these cases, initial mapping of the Antera parameters to the reduced 2D model shows noticeble differences in the reconstructed albedo (center-left column). However, we can see very good agreement between the reconstruction and the photograph using our procedure for adapting and augmenting Antera's parameter maps (center-right column), and even better matching to the photograph using a full 4D search over the parameter space driven by just the albedo map (right column), with softer reconstruction of the albedo similar to the photograph (which has baked-in subsurface scattering). The reconstruction errors (DeltaE94 metric in CIELAB) for various skin patches are reported in Table 2. Thus, either approaches could be used for rendering purposes in many cases with the caveat that our proposed approach for adapting and augmenting Antera's measurements may be more suitable for physiologically motivated simulations than the full 4D search method which tends to better explain the input data, but at the cost of reduced physiological correlation. This can be seen in the back of the hand example in Figure 9, where adapting Antera's maps is unable to model the veins on the hand very well (middle column) as veins are not physiologically explained by melanin and hemoglobin concentration. On the other hand, the full 4D search has enough degrees of freedom to explain the data and better reproduce the appearance of veins in this case but with reduced physiological interpretation of the parameter values.

(a) Photo 1 - normal (b) Photo 2 - flushed (c) Sim. flushing

Figure 10: *Photographs of a female subject acquired under normal (a), and flushed (b) skin conditions. Reconstruction of simulated flushing (c) using spectral parameters estimated under normal condition and applying scaling to the C_h and C_{he} parameters.*

4. Additional Results and Rendering

Figure 10 presents an example of a female subject where she was acquired twice (under W57 illumination), once under normal skin condition (a) and again when her cheeks were rather flushed (b). Given the estimated parameters for her skin from the first acquisition (shown in Figure 8 in the main paper), we scale the corresponding C_h and C_{he} maps to simulate flushing in the cheek area shown in the reconstruction in (c). Here, we employed a manually created mask with edge softening to limit the scaling of the hemoglobin to areas around the cheek. As can be seen, the flushed simulation in (c) produces a reconstruction that is qualitatively quite similar to the photograph of actual flushed skin (b).

4.1. Rendering Subsurface Scattering

In order to render heterogeneous subsurface scattering, we modified the provided subsurface scattering implementation in PBRT from the default dipole diffusion kernel to our specified spatially varying profiles implementing two-layered diffusion. We precompute and store the overall radial reflectance profile due to two-layered diffusion per surface point in linear RGB color space. PBRT framework identifies chromophore parameters mapped to that location and extracts the corresponding precomputed reflectance profile from the tabulated set of all sampled profiles generated with the coloration model for the illumination spectrum. Thereafter, PBRT integrates the selected reflectance profile over radial distances and performs the same operation for all other sampled points on the geometry to add contribution from different spectral profiles, thereby rendering heterogeneous subsurface scattering. The pipeline was implemented by modifying DiffusionReflectance structure from the dipole subsurface integrator, which reads in chromophore fractions and finds the index of spectral reflectance profile within the precomputed tabulated set. Then at runtime, for each generated radial distance from the current point on the surface the distance function will extract the radial profile for the closest sampled point and add it to the overall color contribution, thus integrating the spectral reflectance profile according to geometry and spatial variation in chromophores.

Figure 11 presents corresponding diffuse-only renderings of subjects shown in Figure 1 of the paper, rendered with a point light source with individual spectras of the six types of LEDs on the LED

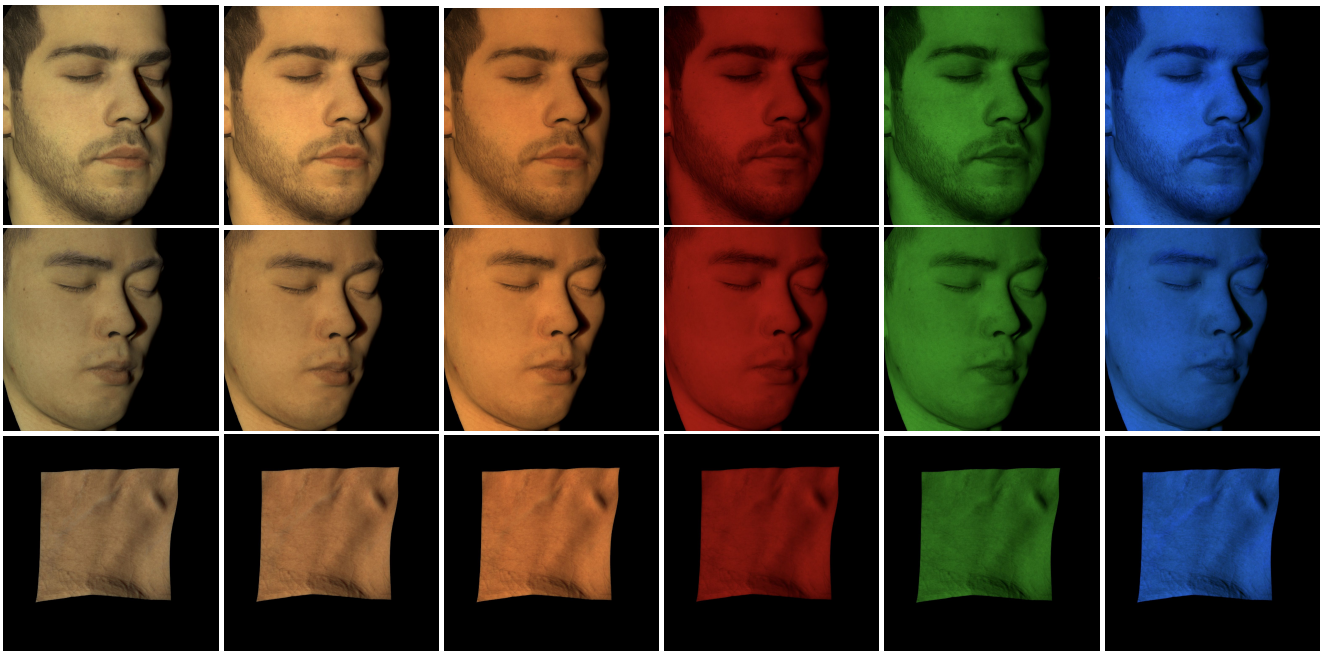

(a) W57 (b) W40 (c) W27 (d) Red (e) Green (f) Blue

Figure 11: *Renderings of acquired faces (top and center row) and a patch of skin (bottom-row) under a point light source with six different LED spectrums (W57, W40, W27, Red, Green and Blue).*

sphere (W57, W40, W27, Red, Green and Blue). Skin appearance change under the various LED spectrums, particularly the softening and reduction of skin texture under the warm white and red illumination respectively, is correctly predicted with our implementation of spatially varying subsurface scattering driven by estimated chromophore maps.

Figure 12 presents a qualitative comparison of our proposed rendering with subsurface scattering (a) against photographs (b) of two male subjects with different skin types (Mediterranian and Asian skin-type respectively) lit with a single point light source (W40 neutral white LED not employed for parameter estimation). Here, the light source in the photographs was cross-polarized with respect to the camera, hence eliminating any specular reflection. We also present a rendering where the spectral parameters have been estimated under a single $D65'$ broadband measurement (c). As can be seen, the renderings have a lot of qualitative similarity with the photographs and well approximate the appearance under a warmer broadband illumination condition. However, the renderings in (a) with joint-estimation under two complementary measurements better preserve skin texture details compared to the renderings in (c) with parameters estimated under a single broadband measurement which encodes a slight blur due to baked-in subsurface scattering.

5. Limitation

The employed 4D skin BSSRDF model is well suited to reconstruct the appearance of skin and facial hair but has limitations and cannot well reconstruct the appearance of domiant veins or tattoos in skin. An example of this can be seen in Figure 13, where skin patches containing veins and a tattoo measured with the Antera device are not well reconstructed even with the full 4D search, and rather poorly reconstructed when using the adapated Antera maps for the reconstruction. This is because veins and tattoos cannot be modeled with melanin and hemoglobin concentrations, which is why Donner et al. [DWd*08] introduced an inter-layer absorption in their model to account for these.

References

[DJ05] DONNER C., JENSEN H. W.: Light diffusion in multi-layered translucent materials. *ACM Transactions on Graphics (TOG) 24*, 3 (2005), 1032–1039. 1

[DJ06] DONNER C., JENSEN H. W.: A spectral bssrdf for shading human skin. In *Proceedings of the 17th Eurographics Conference on Rendering Techniques* (Aire-la-Ville, Switzerland, Switzerland, 2006), EGSR '06, Eurographics Association, pp. 409–417. 1, 2

[DWd*08] DONNER C., WEYRICH T., D'EON E., RAMAMOORTHI R., RUSINKIEWICZ S.: A layered, heterogeneous reflectance model for acquiring and rendering human skin. *ACM Transactions on Graphics (TOG) 27*, 5 (Dec. 2008), 140:1–140:12. 5

[JSB*10] JIMENEZ J., SCULLY T., BARBOSA N., DONNER C., ALVAREZ X., VIEIRA T., MATTS P., ORVALHO V., GUTIERREZ D., WEYRICH T.: A practical appearance model for dynamic facial color. *ACM Transactions on Graphics (TOG) 29*, 6 (Dec. 2010), 141:1–141:10. 1, 2

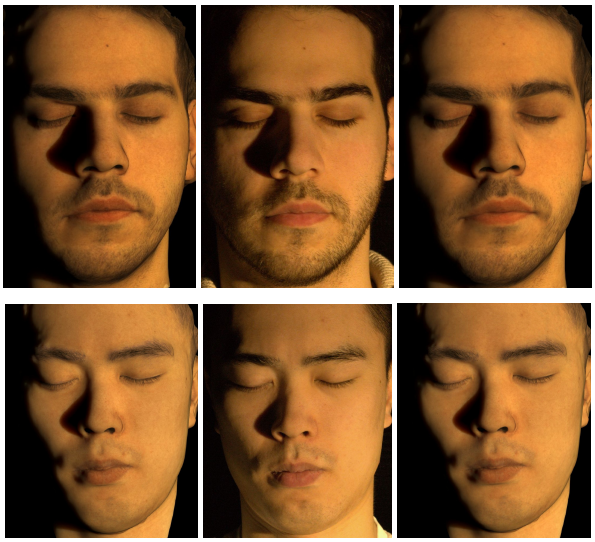

(a) Rendering ($D65'$ + *blue*) (b) Photograph (c) Rendering ($D65'$ only)

Figure 12: *Comparison of our proposed renderings of subsurface scattering with spectral parameters estimated using two complementary measurements (a), against photographs of two different subjects lit with a cross-polarized point light source (W40 LED) (b). (c) Comparison renderings with spectral parameters estimated using a single broadband measurement under* $D65'$.

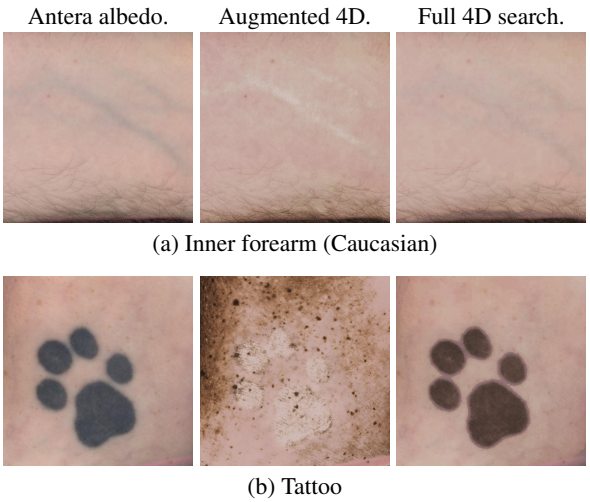

(a) Inner forearm (Caucasian)

(b) Tattoo

Figure 13: *Failure cases for our proposed 4D model and measurement approach. Top-row: Veins in the inner forearm. Bottom-row: Tattoo on the back of neck.*